International Journal of Heat and Mass Transfer 52 (2009) 4375–4385

Contents lists available at ScienceDirect

International Journal of Heat and Mass Transfer

journal homepage: www.elsevier.com/locate/ijhmt

Turbulent open channel flow with heat transfer subjected to the control of a spanwise travelling wave

Nan-Sheng Liu *, Lei Wang, Xi-Yun Lu

Department of Modern Mechanics, University of Science and Technology of China, Hefei, Anhui 230026, PR China

ARTICLE INFO

Article history:
Received 14 July 2008
Received in revised form 1 March 2009
Accepted 30 March 2009
Available online 23 May 2009

Keywords:
Turbulent heat transfer
Lorentz force
Travelling wave
Direct numerical simulation (DNS)
Turbulent open channel flow

ABSTRACT

Turbulent open channel flows with heat transfer subjected to the control of a spanwise travelling wave have been investigated by means of direct numerical simulation (DNS). The three-dimensional Navier–Stokes and energy equations are numerically solved using a fractional-step method. The spanwise travelling wave is induced by a body force that is confined within the viscous layer with its maximum at the bottom wall and decaying exponentially away from it. The objective of this study is to reveal the near-wall turbulence behaviours, the turbulent heat transfer, and thermal structures under the control of the spanwise travelling wave. Three typical frequencies of the spanwise travelling wave, i.e., high-, middle- and low-frequency, corresponding to the exciting periods at $T^+ = 25$, 50 and 100, are investigated to reveal the dynamics of turbulent motions and heat transfer. The Prandtl number (Pr) varies from 1 up to 100. To elucidate the behaviours of turbulence statistics and heat transfer, some typical quantities, including the mean velocity, velocity and vorticity fluctuations, temperature and its fluctuation, turbulent heat fluxes, and the structures of the temperature fluctuation, are exhibited and analyzed.

1. Introduction

The control of wall-bounded flows utilizing a spanwise travelling wave introduced by a body force, e.g., the Lorentz force, is of great interest in applications and fundamentals. Most of existing work [1–9] is aimed to the drag reduction effects induced by the spanwise travelling wave, and to exploiting the relevant mechanisms responsible for the skin friction reduction, e.g., the stabilization and re-organization of near-wall flow structures and the resultant suppression of the turbulence production. To the best of our knowledge, very few studies are concerned about the turbulent heat transfer in the turbulent flow under the control of the spanwise travelling wave. The understanding of the effects of the spanwise travelling wave on the thermal dynamics, especially the turbulent heat fluxes and the thermal structures in the near-wall and free surface regions, is highly desired.

Du et al. [10,11] have proposed the use of a spanwise travelling wave introduced by the Lorentz force to alter the turbulent vortical structures in the wall region, which results in a large amount of drag reduction. According to Du et al. [10,11], an interesting aspect of this new approach is that it enhances the streamwise vortices in the wall region, and leads to the weakening of wall streak intensity and correspondingly the substantial suppression of turbulence production. Another important aspect of this flow control is that the wall streaks are partially stabilized and in many cases most of them are eliminated completely. Both the two aspects make the flow control by using of a spanwise travelling wave quite different from the other traditional drag reduction techniques [12–16]. Although extensive studies have been carried out to reveal the underlying mechanisms of the spanwise travelling wave to reduce the skin friction, there is still never the relevant work documented on its effects on the turbulent open channel flow. This motivates the present authors to investigate the effects of the spanwise travelling wave on the near-wall turbulent motions in the open channel flow.

On the other hand, understanding the effects of the spanwise travelling wave on the turbulent heat transfer in the open channel flow is physically meaningful to the modelling of turbulent Reynolds stress and turbulent heat flux. Some previous work [17–23] indicated that the heat transfer efficiency of the turbulent open channel flow is primarily controlled by the turbulent motions very close to the wall or the free surface. In the free surface region, the flow behaviours are characterized by the surface renewal patches and the hot spots, and the generation of such turbulence structures is mainly dominated by the near-wall turbulent motions [24–29]. Based on these findings, the flow control by use of a spanwise travelling wave is thus expected to have considerable influence on the dynamics of turbulent heat transfer in the open channel flow. Therefore, it is highly tempting to investigate the effects of the spanwise travelling wave on the turbulent motions in the wall region of the turbulent open channel flow and the resultant effects on the thermal dynamics close to the wall and the free surface. However, there is still no study focused on the turbulent heat transfer under the control of the spanwise travelling wave.

* Corresponding author. Tel.: +86 551 3603345; fax: +86 551 3606459.
E-mail address: lns@ustc.edu.cn (N.-S. Liu).

0017-9310/$ - see front matter © 2009 Elsevier Ltd. All rights reserved.
doi:10.1016/j.ijheatmasstransfer.2009.03.072

Nomenclature

F_y	exciting Lorentz force
I	amplitude of the spanwise travelling wave
k	thermal conductivity
Nu_B	Nusselt number at the bottom wall
Nu_F	Nusselt number at the free surface
Pr	Prandtl number
q_W	averaged heat flux through the bottom wall
q_F	averaged heat flux through the free surface
Re_b	Reynolds number based on the bulk mean velocity
Re_τ	Reynolds number based on the friction velocity
t	time
T	temperature
T_L	period of the spanwise travelling wave
T^+, T_L^+	period of the spanwise travelling wave based on the friction velocity
T'	temperature fluctuation
T_B	temperature at the bottom wall
T_F	temperature at the free surface
T_τ	friction temperature
u	streamwise velocity component
u_b	bulk mean velocity
u_i'	velocity fluctuations
u_τ	friction velocity
v	spanwise velocity component
w	vertical velocity component
x	streamwise coordinate
x_i	Cartesian coordinate axes
y	spanwise coordinate
z	vertical coordinate
z_B^+	distance from the bottom wall in viscous unit
z_F^+	distance from the free surface in viscous unit
δ	height of the open channel
Λ	effective penetration length of the Lorentz force excitation
$\Delta z_{\min}^+$	minimum vertical grid size
κ	thermal diffusivity
λ_y	wavelength in the span of the Lorentz force excitation
ν	molecular kinematic viscosity
ω_i'	vorticity fluctuations

Subscripts

rms	root-mean-square

Superscripts

+	normalized quantity by wall parameters
$\langle\rangle$	mean quantity averaged in time and in the horizontal plane

It is our goal of this study to obtain a physical insight into the fundamentals of the turbulent heat transfer and its relationship with the near-wall turbulent motions in the open channel flow, which is subjected to the forcing excitation of a spanwise travelling wave.

In the investigation of the turbulent heat transfer in the open channel flow under the control of a spanwise travelling wave, the difficulties mainly arise from the accurate determination of velocity and temperature fields in the thin thermal boundary layer close to the bottom wall and the interfacial surface, especially in the cases for high-Prandtl number [27–29]. It is well established that direct numerical simulation (DNS) is an effective tool to explore the mechanism of turbulence behaviours and heat transfer, providing in detail the temperature and velocity fluctuations in the wall and surface regions. In this study, the DNS technique is employed to study the effects of the spanwise travelling wave on the near-wall turbulent motions and the resultant turbulent heat transfer in the turbulent open channel flow.

This paper is organized as follows. The mathematical formulations of the turbulent open channel flow with heat transfer, subjected to the control of a spanwise travelling wave, are described in Section 2. The numerical method used and its validations are given in Section 3. In Section 4, some typical statistical turbulence and heat transfer quantities are discussed. Finally, concluding remarks are summarized in Section 5.

2. Mathematical formulations

The three-dimensional incompressible Navier–Stokes and energy equations are used for the DNS of turbulent open channel flow with heat transfer. A body force F_y is introduced into the momentum equations to model the forcing excitation of a spanwise travelling wave exerting on the fluid. To non-dimensionalize the governing equations, the bulk mean velocity u_b is used as the velocity scale, the channel height δ as the length scale, and the temperature difference ΔT between the bottom wall (T_B) and the free surface (T_F) as the temperature scale. The non-dimensional governing equations are given as

$$\frac{\partial u_i}{\partial x_i} = 0 \tag{1}$$

$$\frac{\partial u_i}{\partial t} + \frac{\partial}{\partial x_j}(u_i u_j) = -\frac{\partial p}{\partial x_i} + \frac{1}{\mathrm{Re}_b}\frac{\partial^2 u_i}{\partial x_j \partial x_j} + F_y \delta_{i2} \tag{2}$$

$$\frac{\partial T}{\partial t} + \frac{\partial (T u_j)}{\partial x_j} = \frac{1}{\mathrm{Re}_b \mathrm{Pr}}\frac{\partial^2 T}{\partial x_j \partial x_j} \tag{3}$$

where u_i, T and p are the velocity, temperature and pressure, respectively. In this study, u_i ($i = 1, 2, 3$), for writing convenience, is represented as u, v and w in the streamwise (x), spanwise (y) and vertical (z) directions, respectively. $\mathrm{Re}_b = u_b\delta/\upsilon$ represents the Reynolds number and $\mathrm{Pr} = \upsilon/\kappa$ is the molecular Prandtl number, with υ being the kinematic viscosity and κ the thermal diffusivity.

The spanwise travelling wave modelled by the body force F_y is confined within the viscous sublayer, with its maximum at the bottom wall $z = 0$ and decaying exponentially away from it, as exhibited in Fig. 1. It can be denoted by

$$F_y = I e^{-z/\Delta} \sin\left(\frac{2\pi}{\lambda_y} y - \frac{2\pi}{T_L} t\right) \tag{4}$$

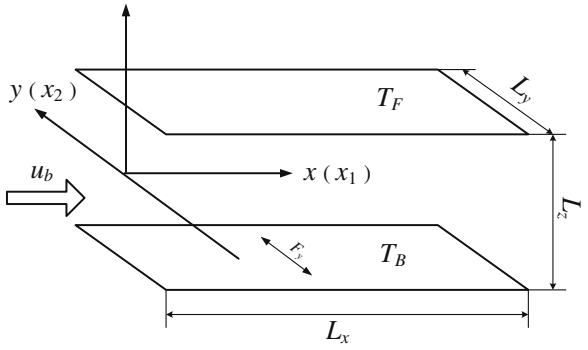

Fig. 1. Sketch of the turbulent open channel flow with heat transfer subjected to the control of a spanwise travelling wave.

where I and Δ represent the amplitude and effective penetration length of the spanwise travelling wave, respectively. λ_y is the wavelength in the span and T_L the period of the spanwise travelling wave.

The present simulations are performed at exciting amplitude $I = 1.36$ and Reynolds number $Re_b = 2300$, corresponding to $Re_\tau = u_\tau\delta/\nu = 150$ approximately, where u_τ is the friction velocity at the bottom wall in the pure shear open channel flow. The Pr number varies from 1 up to 100. The other computational parameters, normalized by the friction velocity u_τ, are chosen to be $\Delta^+ = 3$ and $\lambda_y^+ = 840$, and T_L^+ (denoted by T^+ in the following for simplicity) to be 25, 50 and 100, corresponding to the high-, middle- and low-frequency, respectively.

As shown in Fig. 1 for the sketch of the turbulent open channel flow with heat transfer, no-slip velocity condition is imposed at the bottom wall $z = 0$. Assuming the free surface being absent of significant surface deformation, the boundary conditions applied at $z = 1$, for a shear-free interface without deformation, are given as

$$w = 0, \quad \frac{\partial u}{\partial z} = \frac{\partial v}{\partial z} = 0. \tag{5}$$

The flow and temperature fields are assumed to be statistically homogeneous in the streamwise and spanwise directions. Thus, periodic boundary conditions are employed in these two directions. Two different constant temperatures, i.e., $T_B = 1$ and $T_F = 0$, are imposed on the bottom wall and the free surface, respectively. Heat transfer computation is started after the flow field has statistically reached a fully developed turbulent state. Initial temperature field is set to be a linear distribution along the z-direction and homogeneous in the horizontal plane.

3. Numerical methods

To perform DNS calculation, a fractional-step method proposed by Verzicco and Orlandi [30] is employed to solve Eqs. (1)–(3). Spatial derivatives are discretized by a second-order central difference. Time advancement is carried out by the semi-implicit scheme using the Crank–Nicholson scheme for the viscous terms and the three-stage Runge–Kutta scheme for the convective terms. The discretized formulations were described in detail by Verzicco and Orlandi [30].

In this study, the size of computational domain is set as $7\delta \times 5.6\delta \times \delta$, i.e., half of the two-wall channel height used by Du et al. [11], with the corresponding grid number $128 \times 128 \times 192$ in the streamwise, spanwise and vertical directions, respectively. The grid is uniform along the streamwise and spanwise directions. In the vertical direction, to increase the grid resolution near the free surface and the wall, the mesh is stretched with a transformation used in [23,25], so that the minimum vertical grid sizes about $\Delta z_{min}^+ = 0.1$, 0.06 and 0.03 are used for Pr = 1, 10 and 100, respectively. According to Bergant and Tiselj [31], the grid system used is ensured to be capable of resolving all the essential scales of turbulence, with the smallest resolved temperature scales equal to the smallest scales of the velocity field for high-Pr calculations. The grid independence has been ensured for every simulation in the present study [32].

To validate the numerical method and computational code used, DNS of the turbulent two-wall channel flow at $T^+ = 50$ has been carried, in which the fluid in the bottom wall region is controlled by the spanwise travelling wave. Fig. 2a shows the logarithm profiles of mean velocity (i.e., $\langle u^+ \rangle$) near the controlled (bottom) and uncontrolled (top) walls, comparing well with the results of Du et al. [11]. Here, z^+ denotes the distance in viscous unit from the controlled wall for the velocity profile near the controlled wall, or the distance from the uncontrolled wall for the velocity profile near the uncontrolled wall. The three components of turbulence intensity, rescaled by the centre-line velocity, are plotted in

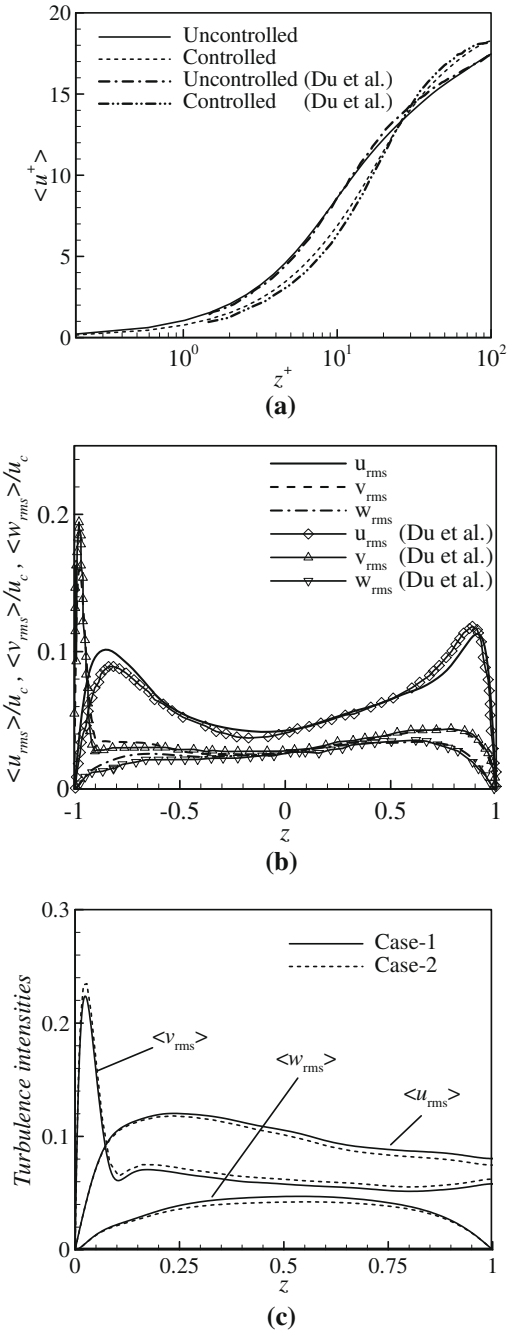

Fig. 2. Turbulence statistics of the two-wall channel flow at $T^+ = 50$ and comparisons with previous results: (a) mean velocities and (b) turbulence intensities. (c) Comparison of turbulence intensities obtained by different computational domain sizes for the open channel flow at $T^+ = 50$. Here, Case-1 denotes the calculation by $7\delta \times 5.6\delta \times \delta$ with grid number $128 \times 128 \times 192$, and Case-2 by $14\delta \times 11.2\delta \times \delta$ with grid number $256 \times 256 \times 192$ in the streamwise, spanwise and vertical directions, respectively.

Fig. 2b, exhibiting good agreements with those obtained by Du et al. [11]. Other typical turbulent quantities and wall structures also agree well with the results in Ref.[11] in our detailed test simulations [32]. Moreover, the present computational code has been verified extensively in our previous work [23–27]. Here, to ensure the independence of computational domain size, turbulence intensities obtained by different computational domain sizes for the open channel flow at $T^+ = 50$ are typically given in Fig. 2c, which indicates the little influence of the computational domain size on

the turbulence statistics. Thus, the results obtained by $7\delta \times 5.6\delta \times \delta$ are used to deal with the flow behaviours. In summary, it can be ensured that our calculation is reliable to predict the statistical quantities of turbulent flow under the forcing excitation of the spanwise travelling wave.

4. Results and discussion

4.1. Drag reduction and turbulence statistics

Turbulent open channel flows under the control of the spanwise travelling wave at $T^+ = 25$, 50 and 100, corresponding to the high-, middle- and low-frequency regimes, respectively, are simulated to reproduce the drag reduction and to examine the effects of the forcing excitation on the near-wall turbulent motions.

The time series of the shear stress at the bottom wall, scaled by the wall shear stress in the pure shear open channel flow (no-control case), are exhibited in Fig. 3 for different spanwise travelling waves. Even qualitatively, the results indicate a strong dependence of drag reduction on the exciting period of the spanwise travelling wave. The travelling-wave-induced reduction of skin friction in the present DNS simulations is in rational agreement with those in Ref.[11]. The high-frequency excitation at $T^+ = 25$ gives a considerable drag reduction reaching about 15%, and in the middle-frequency case for $T^+ = 50$ it leads to the maximum drag reduction among the three cases, which is more than 30%; however, the low-frequency excitation at $T^+ = 100$ results in the drag augmentation. Further, the time evolutions of the drag force obtained in the present calculations are similar to those in Ref.[11] for all the spanwise travelling waves. These desirable results also ensure that the present calculations are accurately reliable.

Fig. 4 depicts the profiles of mean velocity at different exciting periods, scaled by the friction velocity u_τ, where z_B^+ is the distance from the bottom wall in viscous unit. In the wall region, the mean velocity $\langle u^+ \rangle$ decreases in the cases of drag reduction (i.e., at $T^+ = 25$ and 50). This trend of $\langle u^+ \rangle$ leads to the thickening of viscous sublayer and the consequential decrease of skin friction at the bottom wall, as predicted in Fig. 3. As T^+ increases up to 100, $\langle u^+ \rangle$ increases slightly and overrides that of no-control flow within the viscous sublayer, indicating the increase of skin friction with respect to the pure shear open channel flow. Fig. 4 also shows the increase of $\langle u^+ \rangle$ near the free surface ($z = 1$) and the thinning of the log-law region under the high- and middle-frequency excitations, i.e., at $T^+ = 25$ and 50. This feature of $\langle u^+ \rangle$ is resulted from the drag reduction at the bottom wall and leads to the slight increase of shear stress in the vicinity of the free surface. While subjected to the low-frequency travelling wave (i.e., at $T^+ = 100$), $\langle u^+ \rangle$ decreases

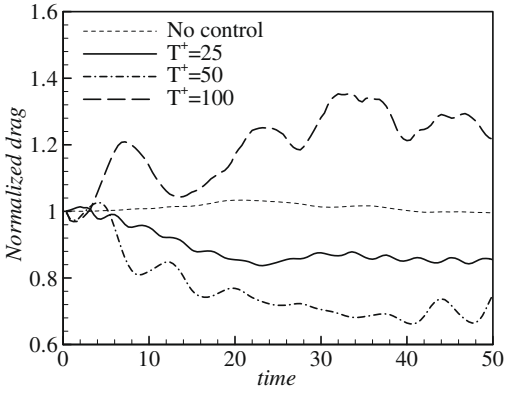

Fig. 3. Time series of normalized skin friction for different spanwise travelling waves.

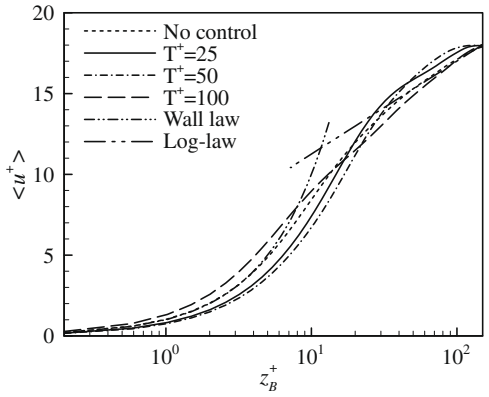

Fig. 4. Logarithm profiles of mean velocity for different spanwise travelling waves.

in the free surface region and the thickening of log-law region is attributed to the drag augmentation at the bottom wall.

The profiles of the three components of turbulence intensity, i.e., the root-mean-square (rms) of velocity fluctuation, are plotted in Fig. 5 to examine the turbulence behaviour in response to the spanwise travelling wave. Due to the fact that the wall shear process of main flow is mainly responsible for the production of the streamwise turbulence fluctuation [24–26,33], the trend of the streamwise turbulence intensity (i.e., $\langle u_{rms} \rangle$) should be consistent with that of the shear stress in the wall region. As expected, Fig. 5a shows the considerable decrease of $\langle u_{rms} \rangle$ subjected to the high- and middle-frequency travelling waves (i.e., at $T^+ = 25$ and 50) in the wall region, as well as its remarkable increase in the case of low-frequency excitation (i.e., at $T^+ = 100$). This observation of $\langle u_{rms} \rangle$ suggests that the turbulent production of the streamwise velocity fluctuation is suppressed in the drag reduction cases and agitated in the drag augmentation case. When the maximum drag reduction is achieved at $T^+ = 50$, $\langle u_{rms} \rangle$ presents the lowest local maximum in the wall region among all the three cases, indicating the greatest suppression of bursting events to generate the streamwise turbulence fluctuation; while in the region near the free surface, $\langle u_{rms} \rangle$ increases due to the increase of the mean velocity gradient (i.e., the shear stress), as indicated in Fig. 4. Different from the no-control open channel flow, the forcing excitation induces a spanwise fluid motion in the vicinity of the controlled wall, which is enhanced with the frequency decrease of the spanwise travelling wave [11]. The resultant shear process of the travelling-wave-induced spanwise fluid motion contributes remarkably to the generation of the spanwise turbulence fluctuation. Consequently, another important effect of the spanwise travelling wave is to increase $\langle v_{rms} \rangle$ greatly near the bottom wall, as seen in Fig. 5b. It is also exhibited in Fig. 5b that $\langle v_{rms} \rangle$ almost remains unaltered in the region close to the free surface, indicating that the spanwise velocity fluctuation suffers little influence from the travelling-wave-induced spanwise fluid motion near the bottom wall. In Fig. 5c, $\langle w_{rms} \rangle$ decreases considerably in the wall region for the spanwise travelling wave at $T^+ = 25$ then increases greatly when the exciting period T^+ increases to 50 and 100. This observation suggests that the vertical turbulence fluctuation is mainly generated by the energy redistribution process linked to the main flow in the case of high-frequency excitation and by that linked to the travelling-wave-induced spanwise fluid motion in the case of low-frequency excitation [25,34].

Fig. 6 shows the profiles of three components of vorticity fluctuation to reveal the near-wall vorticity fluctuations subjected to the spanwise travelling wave. The streamwise vorticity fluctuation $\langle \omega_{x\,rms} \rangle$ in Fig. 6a is enhanced significantly in the region immediately close to the bottom wall, as the exciting period increases from

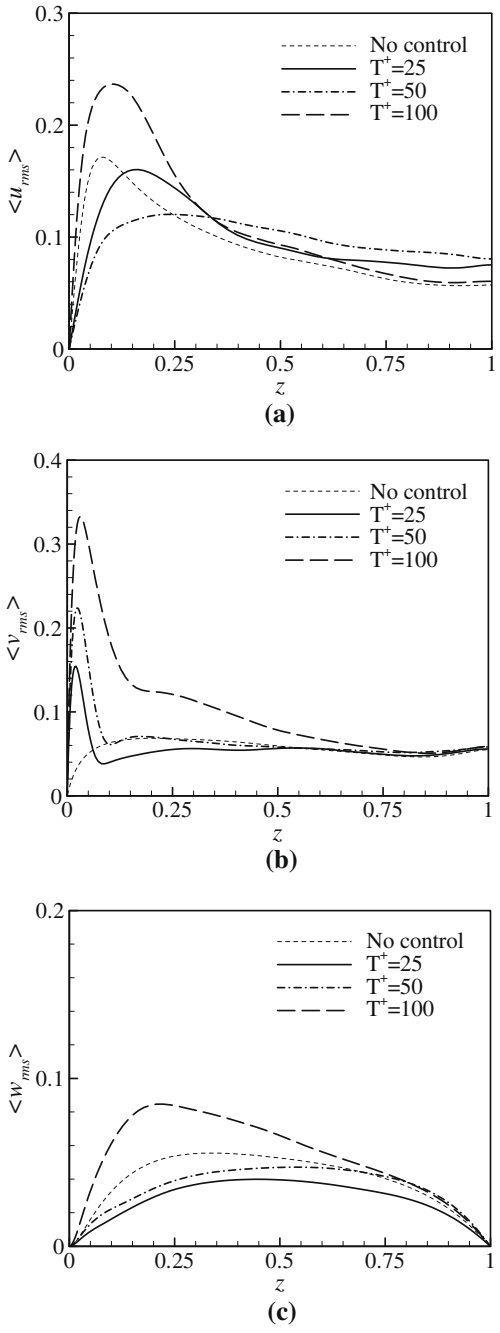

Fig. 5. Profiles of turbulence intensities: (a) streamwise, (b) spanwise and (c) vertical components, normalized by the centre-line velocity.

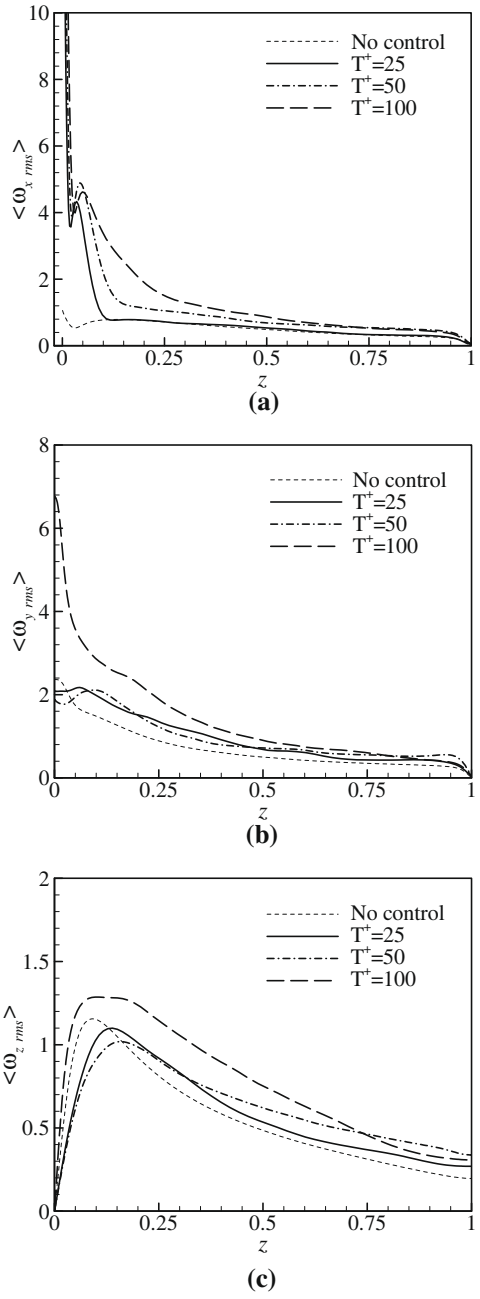

Fig. 6. Profiles of vorticity fluctuations: (a) streamwise, (b) spanwise and (c) vertical components, scaled by the centre-line velocity.

$T^+ = 25$ up to 100. This trend of $\langle \omega_{x\ rms} \rangle$ is attributed to the shear process of the travelling-wave-induced spanwise fluid motion, which is enhanced with the frequency decrease of the forcing excitation and contributes to the production of the streamwise vorticity fluctuation [35]. As seen in Fig. 6b, the spanwise vorticity fluctuation (i.e., $\langle \omega_{y\ rms} \rangle$), which is linked to the elongated wall streaks in the wall region [33,36], decreases slightly at the bottom wall in the high- and middle-frequency regimes (i.e., at $T^+ = 25$ and 50) but increases greatly in the low-frequency regime (i.e., at $T^+ = 100$). This observation indicates that the wall streaky structures are gradually suppressed in the cases of drag reduction (i.e., at $T^+ = 25$ and 50), but enhanced remarkably in the case of drag augmentation (i.e., at $T^+ = 100$). In Fig. 6c, the vertical vorticity fluctuation (i.e., $\langle \omega_{z\ rms} \rangle$) exhibits the same tendency as that of $\langle u_{rms} \rangle$ in the vicinity of the controlled wall. It is due to the fact that the vertical vorticity fluctuation is mainly generated by the shear process linked to the main flow [36].

4.2. Temperature and thermal statistics

In the present study, turbulent open channel flows with Pr ranging from 1 up to 100 are simulated to investigate the effects of the spanwise travelling wave on the dynamics of turbulent heat transfer. Here, special interests are devoted to the thermal behaviours at low- and high-Prandtl numbers, i.e., Pr = 1 and 100, respectively. In Fig. 7, the mean temperature profiles are plotted logarithmically to emphasize the behaviours near the wall for Pr = 1 and 100, where $\langle T \rangle^m$ is defined as $\langle T \rangle^m = T_B - \langle T \rangle$. Similar to the trend of $\langle u^+ \rangle$ in Fig. 4, $\langle T \rangle^m$ decreases in the diffusive layer under

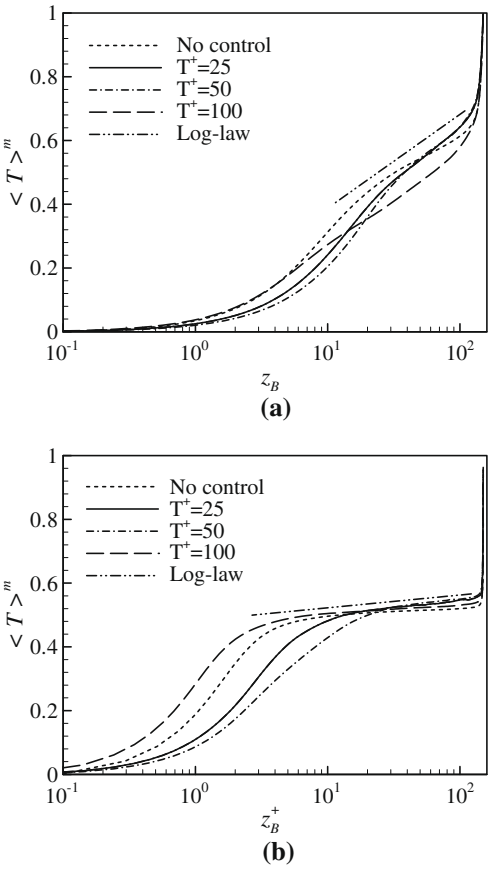

Fig. 7. Mean temperature normalized by the friction temperature for: (a) Pr = 1 and (b) Pr = 100, where $\langle T\rangle^m = T_B - \langle T\rangle$.

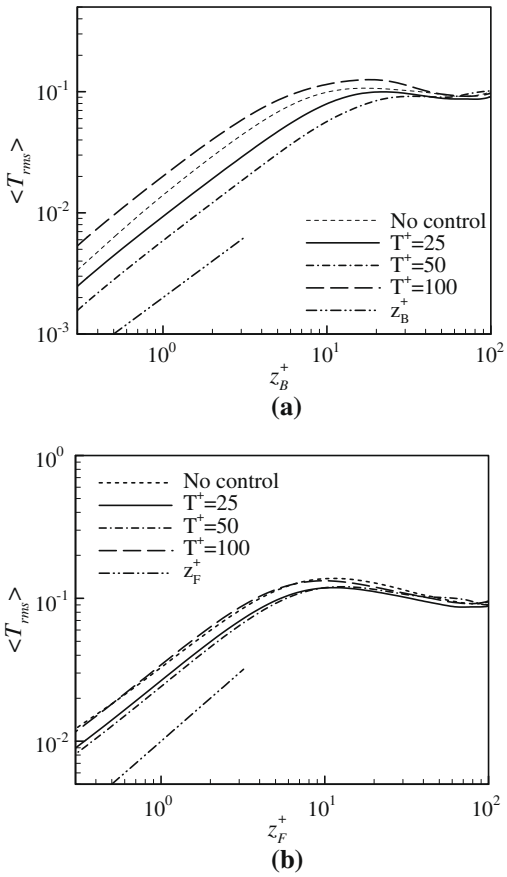

Fig. 8. Temperature fluctuations for Pr = 1: (a) near the wall and (b) near the free surface.

the high- and middle-frequency excitations (i.e., at $T^+ = 25$ and 50), while increases in the low-frequency case (i.e., at $T^+ = 100$). This behaviour of $\langle T\rangle^m$ is responsible for the thickening of the thermal diffusive layer in the cases of drag reduction and its thinning in the case of drag augmentation. As exhibited in Fig. 7, there also exists in the mean temperature profile a buffer layer followed by a logarithmic region, whose slope is interestingly independent of the exciting frequency of the spanwise travelling wave for a fixed Prandtl number. This feature of the mean temperature profile was also found in the turbulent flow with heat transfer involving other flow control methods [26,27]. For Pr = 1 in Fig. 7a, it is seen that the mean temperature profiles suffer considerable influence from the forcing excitation even in the log-law region near the free surface. While for Pr = 100 in Fig. 7b, only in the near-wall region do the temperature profiles exhibit strong dependence on the spanwise travelling wave; however, little influence of the forcing excitation on the mean temperature profiles is identified out of the buffer layer. This observation is due to the fact that the heat transfer process mainly occurs within the very thin diffusive sublayer close to the bottom wall in the turbulent flow for high-Prandtl number [27].

The temperature fluctuations (i.e., $\langle T_{rms}\rangle$) near the bottom wall (Fig. 8a) and the free surface (Fig. 8b) for Pr = 1 both show the same tendencies as that of $\langle u_{rms}\rangle$ in Fig. 5a, decreasing in the drag reduction cases (i.e., at $T^+ = 25$ and 50) and increasing in the drag augmentation case (i.e., at $T^+ = 100$). Here, z_F^+ denotes the distance from the free surface in viscous unit. This observation confirms the fact that the dynamic process to generate temperature fluctuation is closely linked to the bursting events in the wall region and to the resultant surface renewal events near the free surface [17–23]. In the vicinity of the wall (or free surface), the temperature fluctuation can be represented by the following expansion series [37], in terms of z_B^+ (or z_F^+),

$$T_{rms} = a_{B1}z_B^+ + a_{B2}z_B^{+2} + \cdots \quad \text{near the wall} \tag{6a}$$

$$T_{rms} = a_{F1}z_F^+ + a_{F2}z_F^{+2} + \cdots \quad \text{near the free surface} \tag{6b}$$

Usually, the expansion coefficients are functions of the relevant parameters (e.g., Pr and T^+ here). As shown in Fig. 8, for the open channel flow under the control of the spanwise travelling wave, the expansions of Eq. (6) can be confirmed based on the agreement of leading terms in Eq. (6) with the profiles of $\langle T_{rms}\rangle$ in the wall and free surface regions. Interestingly, the profiles of temperature fluctuation scaled by the friction temperature T_τ, i.e., $\langle T^+_{rms}\rangle$, if renormalized by the Prandtl number Pr, almost collapse into each other in the diffusive sublayer for all the spanwise travelling waves, as depicted in Fig. 9. This feature of $\langle T^+_{rms}\rangle$ was also found in our previous work involving other flow control methods [23,27].

Fig. 10 shows the streamwise and spanwise components of turbulent heat flux, i.e., $\langle T'u'\rangle$ and $\langle T'v'\rangle$, near the wall and the free surface for Pr = 1 and 100. Similarly, $\langle Tu'\rangle$ and $\langle Tv'\rangle$ can be also expressed as power series of z_B^+ and z_F^+ near the boundaries [23,27],

$$\langle T'u'\rangle(\text{or } \langle T'v'\rangle) = a_1z_B^{+2} + a_2z_B^{+3} + \cdots \quad \text{near the wall} \tag{7a}$$

$$\langle T'u'\rangle(\text{or } \langle T'v'\rangle) = b_1z_F^+ + b_2z_F^{+2} + \cdots \quad \text{near the free surface} \tag{7b}$$

Then, both curves of the square and linear laws, via the vertical distance z_B^+ and z_F^+, respectively, are plotted in Fig. 10 with logarithmic scales to illustrate the first terms in Eq. (7). Although subjected to the spanwise travelling wave, the turbulent heat fluxes in the

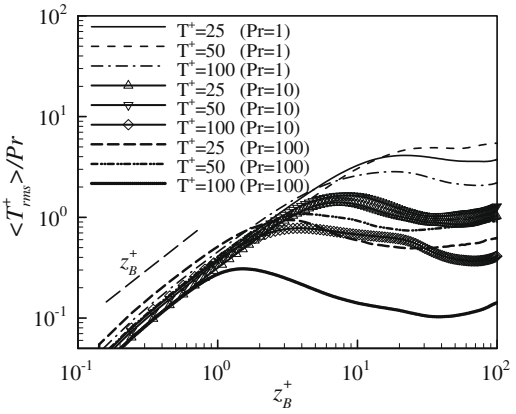

Fig. 9. Renormalized temperature fluctuations for different Prandtl numbers near the wall.

streamwise and spanwsie directions are still in good agreement with the leading terms in Eq. (7) near the boundaries. As seen in Fig. 10a and c, $\langle T'u'\rangle$ follows the trend of $\langle u_{rms}\rangle$ both in the vicinity of bottom wall and in that of free surface. Considering the view of Fig. 5a, this observation indicates the dominance of the streamwise turbulence fluctuation on the dynamics process of turbulent heat transfer linked to $\langle T'u'\rangle$. Differently, $\langle T'v'\rangle$ exhibits the same tendency as that of $\langle v_{rms}\rangle$ in the wall region (Fig. 10b), increasing monotonically as the spanwise travelling wave varies from high- to low-frequency regimes, i.e., from $T^+ = 25$ to 100; but in the vicinity of free surface (Fig. 10d), $\langle T'v'\rangle$ decreases in the drag reduction cases at $T^+ = 25$ and 50, then increases in the drag augmentation case at $T^+ = 100$, consistent with the tendency of $\langle T_{rms}\rangle$ in Fig. 8b. Thus, the turbulent heat transfer linked to $\langle T'v'\rangle$ is dominated by the spanwise turbulence fluctuation linked to the travelling-wave-induced spanwise fluid motion near the bottom wall; but in the free surface region, it is dominated by the temperature fluctuation linked to the surface renewal events originating from the buffer layer of the bottom wall [23].

The Nusselt number is an important parameter relevant to the heat transfer efficiency for the turbulent flow, which is defined as

$$\mathrm{Nu}_B = \frac{q_W \delta}{k\Delta T} \quad \text{and} \quad \mathrm{Nu}_F = \frac{q_F \delta}{k\Delta T} \tag{8}$$

at the bottom wall and the free surface, respectively. Here, q_W and q_F represent the averaged heat flux through the bottom wall and the free surface, respectively; k is the thermal conductivity. Fig. 11 shows the Nusselt number versus Pr for different spanwise travelling waves. For a given Prandtl number, Nu decreases in the drag reduction cases at $T^+ = 25$ and 50, however increases in the drag augmentation case at $T^+ = 100$, both at the bottom wall (Fig. 11a) and at the free surface (Fig. 11b). This observation indicates that the turbulent heat transfer is weakened in the drag reduction cases due to the turbulence suppression; but enhanced as a result of the turbulence agitation when the skin friction increases.

To validate the present predictions, Fig. 11 also exhibits the well accepted $\mathrm{Pr}^{1/3}$-law at the solid wall and $\mathrm{Pr}^{1/2}$-law at the free surface for comparison. In Fig. 11a, it is confirmed that the distribution of Nu is well related to the law $\mathrm{Pr}^{1/3}$ at the bottom wall as Pr varies from 1 up to 100. In Fig. 11b, the calculated Nu at the free surface are compared with the gas flux measurements of Komori et al. [17] and the empirical correlation developed by Rashidi et al. [20]. They correlated their experimental results with the subsurface hydrodynamics with the aid of the surface renewal approximation. The correlations can be normalized using only the Reynolds and Prandtl numbers as

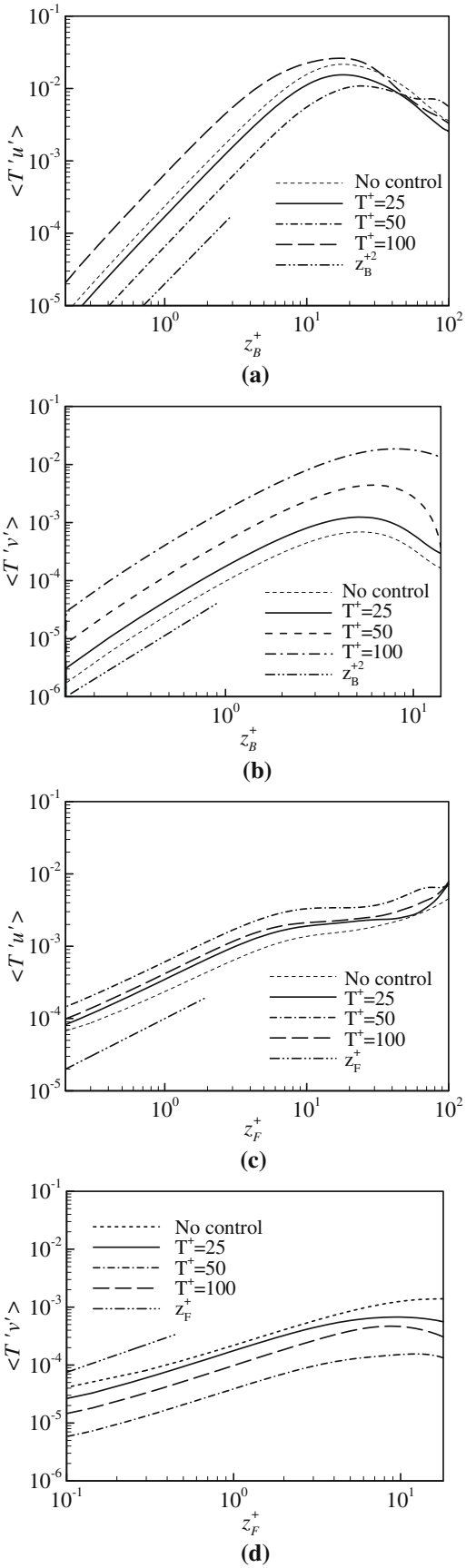

Fig. 10. Turbulent heat fluxes near the wall: (a) streamwise and (b) spanwise components; and turbulent heat fluxes near the free surface: (c) streamwise and (d) spanwise components.

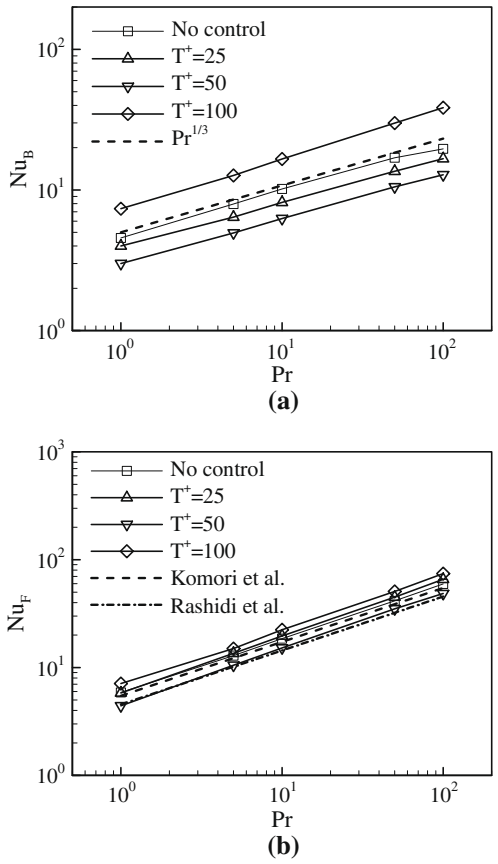

Fig. 11. Nusselt number versus the Prandtl number: (a) near the wall and (b) near the free surface; and the comparisons with the corrections proposed by Komori et al. [17] and Rashidi et al. [20].

$$\mathrm{NuPr}^{-1/2} = 4.21 \times 10^{-3}\mathrm{Re}_b^{0.927} \quad \text{(Komori et al.17)} \tag{9a}$$

$$\mathrm{NuPr}^{-1/2} = 3.22 \times 10^{-3}\mathrm{Re}_b^{0.938} \quad \text{(Rashidi et al.20)} \tag{9b}$$

Fig. 11b shows rational agreement of the present predictions with the correlations given by Eq. (9). As the unavoidable experimental errors are considered, the present Nu predictions are acceptably reliable. Further, the comparisons in Fig. 11 also indicate clearly that the correlations in Eq. (9) must be modified to be feasible for the prediction of Nu in the open channel flows with heat transfer subjected to the control of the spanwise travelling wave.

4.3. Structures of the temperature fluctuation

To examine the influence of the spanwise travelling wave on the turbulent heat transfer in the open channel flow, the structures of the temperature fluctuation near the wall and the free surface are exhibited and briefly analyzed in the following for the low- and high-Prandtl number cases (i.e., Pr = 1 and 100).

Fig. 12 shows the contours of the instantaneous temperature fluctuation in the horizontal plane near the bottom wall ($z_B^+ = 5$) for Pr = 1 and 100. Similar to the streamwise velocity fluctuation [11], the temperature fluctuation in Fig. 12 for Pr = 1 is suppressed in the drag reduction cases at $T^+ = 25$ and 50; while agitated in the drag augmentation case at $T^+ = 100$. This observation is in good agreement with the trend of $\langle T_{rms}\rangle$ in Fig. 8a. Interestingly, the effects of the spanwise travelling wave gradually eliminate the elongated thermal streaks and give birth to the wide zones of high- and low-temperature fluids, resembling a spanwise travelling wave. As the forcing excitation varies from high- to low-frequency regimes, the spanwise spacing of the thermal streaks becomes larger, especially in the low-frequency case at $T^+ = 100$. The thermal structures for Pr = 100 exhibit the trend similar to that for low-Prandtl number under the influence of the spanwise travelling wave. As reported, the scale of temperature fluctuation decreases with the increase of Pr in a manner inversely proportional to $\mathrm{Pr}^{1/2}$ [38]. Therefore, the scale of thermal structures for Pr = 100 is reasonably found to be relatively small in Fig. 12, but the intensity of temperature fluctuation increases evidently compared to the low-Pr case.

About 90% of bursting eddies generated in the boundary layer of wall turbulence evolve into the surface-renewal motions [17], and contribute to the formation of hot spots near the free surface by the splattering events [22,23]. Thus, the behaviour of the surface thermal structures is expected to be consistent with the profiles of the streamwise turbulence intensity. As indicated in Fig. 13 for Pr = 1, the intensity of hot spots near the free surface decreases in the drag reduction cases at $T^+ = 25$ and 50; then increases in the drag augmentation case at $T^+ = 100$. This observation of the thermal structures agrees well with the trend of $\langle u_{rms}\rangle$ shown in Fig. 5a. To be noted, Fig. 13 exhibits no temperature structures in the form of the spanwise travelling wave in the free surface region. This reasonable observation confirms that the temperature structures in the free surface region only link to the spanwise travelling wave confined in the wall region by the resultant turbulence events, i.e., bursting events in the wall region and renewal events near the free surface [24–29]. In Fig. 13, fairly dense thermal structures arise at high-Pr number (i.e., Pr = 100), but no evident modification of the temperature structure pattern is visualized near the free surface when the spanwise travelling wave changes from high- to low-frequency regimes. It is due to the fact that the dynamic process of turbulent heat transfer only occurs in the very thin diffusive layer near the bottom wall for high-Prandtl number. Consequently, the influence of the spanwise travelling wave could not reach the free surface by the bursting eddies in the wall region, which carry the high- and low-temperature fluids towards the free surface.

In Fig. 14, the near-wall contours of the instantaneous temperature fluctuation, in a cross plane (y, z_B^+) for Pr = 1 and 100, exhibit the coherent structures due to the succession of ejection and sweeping events. The overview of Fig. 14 clearly shows the presence of the wide zones of high- and low-temperature structures in the wall region, and the gradual increase of its spanwise spacing with the frequency decrease of the spanwise travelling wave. In the cases at low-Prandtl number, the closed contours of temperature fluctuation exhibit streaky structures with large vertical scale even more than $z_B^+ = 40$, it suggests that the near-wall temperature structures can be carried into the free surface region by the ejection events; then give birth to the hot spots there by the splattering events. In contrast, the vertical scale of temperature structures is relatively small in the wall region for Pr = 100, indicating that the turbulent heat transfer process meanly occurs within a very thin layer immediately close to the wall.

5. Concluding remarks

Direct numerical simulations of the turbulent open channel flow with heat transfer are carried out to reveal the effects of the spanwise travelling wave on the characteristics of turbulent motions, turbulent heat transfer, and temperature structures. As indicated by the time evolutions of skin friction, the present work reproduces the drag reduction under the high- and middle-frequency excitations (i.e., at $T^+ = 25$ and 50) and the drag augmentation for the low-frequency excitation (i.e., at $T^+ = 100$). In the drag reduction cases, the streamwise turbulence intensity, as well as the vorticity fluctuations in the spanwise and vertical directions, decreases due to the suppression of turbulence events in the wall

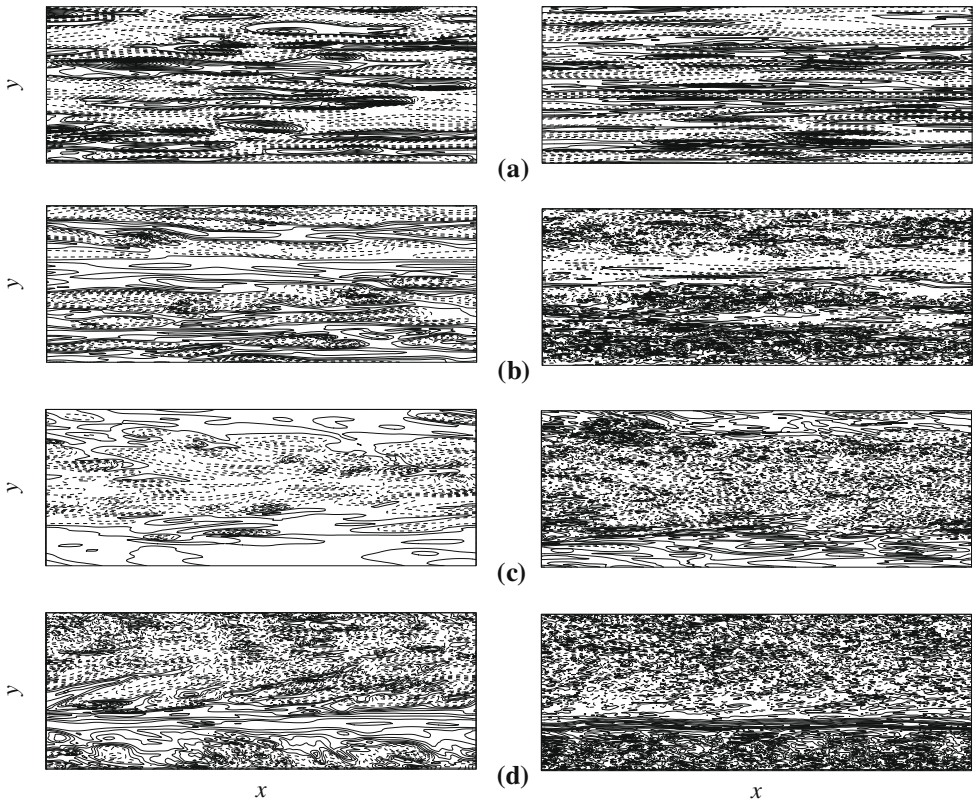

Fig. 12. Contours of the instantaneous temperature fluctuation near the wall ($z_B^+ = 5$) for Pr = 1 (left column) and Pr = 100 (right column) for different spanwise travelling waves: (a) no control; (b) $T^+ = 25$; (c) $T^+ = 50$ and (d) $T^+ = 100$. Here, increment of temperature fluctuation is 0.05.

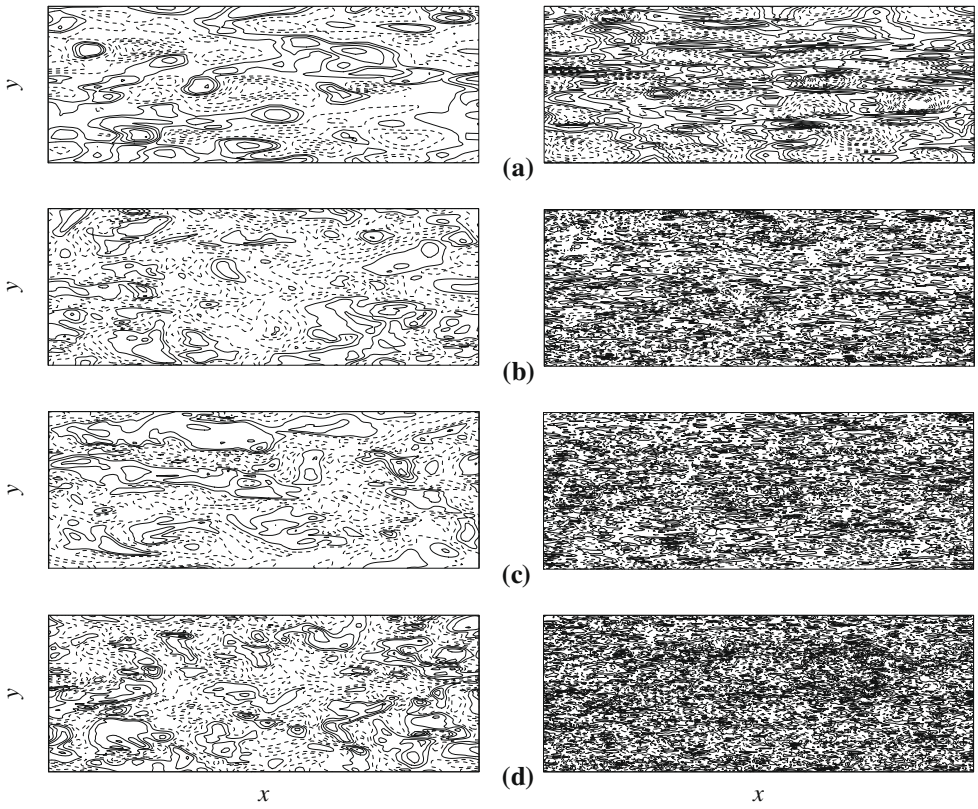

Fig. 13. Contours of the instantaneous temperature fluctuation near the free surface ($z_F^+ = 5$) for Pr = 1 (left column) and Pr = 100 (right column) for different spanwise travelling waves: (a) no control; (b) $T^+ = 25$; (c) $T^+ = 50$ and (c) $T^+ = 100$. Here, increment of temperature fluctuation is 0.1.

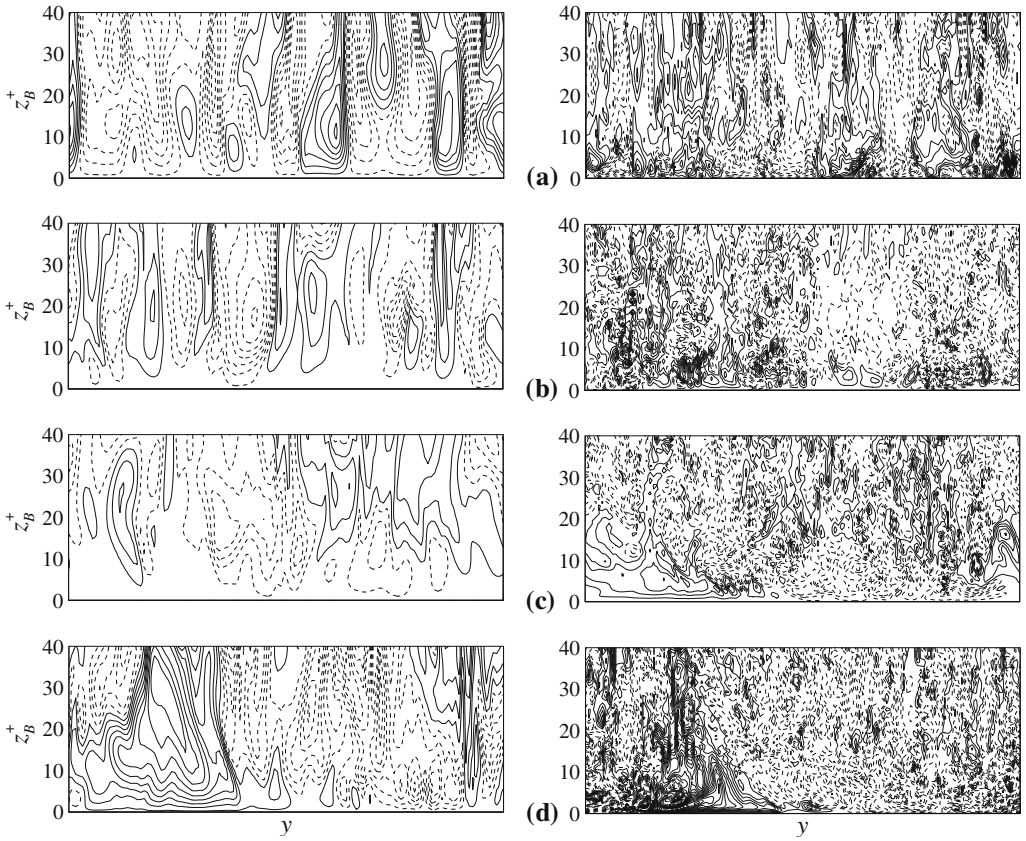

Fig. 14. Contours of the instantaneous temperature fluctuation in the (y, z_B^+) plane for Pr = 1 (left column) and Pr = 100 (right column) for different spanwise travelling waves: (a) no control; (b) $T^+ = 25$; (c) $T^+ = 50$ and (d) $T^+ = 100$. Here, increment of temperature fluctuation is 0.05.

region; in the drag augmentation case, the control of the spanwise travelling wave leads to considerable increase of the turbulence statistics mentioned above. An important effect of the spanwise travelling wave is to enhance the turbulence statistics linked to the spanwise turbulence fluctuation, by the shear process of the travelling-wave-induced spanwise fluid motion in the wall region, which is augmented with the frequency decrease of the forcing excitation. As the results, the spanwise and vertical turbulence intensities, as well as the streamwise and spanwsie vorticity fluctuations, increase obviously close to the wall, especially under the low-frequency excitation at $T^+ = 100$.

When heat transfer is considered in the turbulent open channel flow for Pr = 1 and 100, the dynamics of turbulent heat transfer is mainly dominated by the turbulence events in the wall region. The mean temperature, the temperature fluctuation and the streamwise turbulent heat flux, in the vicinities of bottom wall and free surface, exhibit the trends exactly similar to that of streamwise turbulence intensity, increasing in the drag reduction cases while decreasing in the drag augmentation case. Differently, the behaviour of the spanwise turbulent heat flux is consistent with that of the spanwise turbulence fluctuation in the wall region, indicating the dominance of travelling-wave-induced spanwise fluid motion there; but near the free surface, it is similar to that of the temperature fluctuation, therefore the dynamics of spanwise turbulent heat flux in the free surface region is dominated by the surface renewal events. The prediction of Nu numbers at the bottom wall and the free surface indicates the weakening of heat transfer in the drag reduction cases and its agitation in the drag augmentation case, due to the effects of the spanwise travelling wave.

Based on the contours of the instantaneous temperature fluctuation for Pr = 1 and 100, the wide zones of high- and low-temperature structures, in form of a spanwise travelling wave, are clearly identified in the wall region, whose spanwise spacing increases gradually as the spanwise travelling wave changes from high- to low-frequency. Near the free surface, temperature structures suffer little influence from the control of the spanwise travelling wave; the hot spots in the free surface region are mainly generated by the splattering events linked the bursting eddies in the wall region, which eject the high- and low-temperature fluid towards the free surface. For the turbulent flow at high-Prandtl number, the dynamic process of turbulent heat transfer mainly occurs in the very thin diffusive layer immediately close to the wall.

Acknowledgements

This work was supported by the National Natural Science Foundation of China (Nos. 10772173, 90405007 and 90605005), the Science and Technology Innovative Foundation of the Chinese Academy of Sciences (No. CXJJ237) the Anhui Province Excellent Young Scholars Foundation (No. 8416826).

References

[1] D.M. Nosenchuck, G.L. Brown, Discrete spatial control of wall shear stress in a turbulent boundary layer, in: C.G. Speziale, B.E. Launder (Eds.), Proc. of the Intl. Conf. on Near-Wall Turbulent Flows, Tempe, Arizona, 1993.
[2] C. Henoch, J. Stace, Experimental investigation of a salt water turbulent boundary modified by an applied streamwise magnethydrodynamic body force, Phys. Fluids 7 (1995) 1371–1383.
[3] D.M. Nosenchuck, Boundary layer control using the Lorentz force, in: Proc. of the ASME Fluid Engineering Meeting, San Diego, July 7–11, 1996.
[4] P.R. Bandyopadhyay, J.M. Castano, Micro-tiles for electromagnetic turbulence control in saltwater-preliminary investigations, in: Proc. of the Symp. on Turbulence Modification and Drag reduction, ASME Summer Meeting, 1996.

[5] C.H. Crawford, G.E. Karniadakis, Reynolds stress analysis of EMHD-controlled wall turbulence. Part I, Phys. Fluids 9 (1997) 788–806.
[6] P.L. O'Sullivan, S. Biringen, Direct numerical simulations of low Reynolds number turbulent channel flow with EMHD control, Phys. Fluids 10 (1998) 1169–1181.
[7] Y.Q. Du, Paralled DNS of electro-magnetic flow control, Ph.D. Thesis, Brown University, 1999.
[8] Y.Q. Du, A. Beskok, G.E. Karniadakis, Simulation of a Lorentz force actuator, in: Proc. of the 3rd ASME/JSME Joint Fluids Engineering Conference, San Fransisco, CA, July 18–22, 1999.
[9] T.W. Berger, J. Kim, C. Lee, J. Lim, Turbulent boundary control utilizing the Lorentz force, Phys. Fluids 12 (2000) 631–649.
[10] Y.Q. Du, G.E. Karniadakis, Suppressing wall turbulence by means of a transverse travelling wave, Science 288 (2000) 1230–1234.
[11] Y.Q. Du, V. Symeonidis, G.E. Karniadakis, Drag reduction in wall-bounded turbulence via a transverse travelling wave, J. Fluid Mech. 457 (2002) 1–34.
[12] W.J. Jung, N. Mangiavacchi, R. Akhavan, Suppression of turbulence in wall-bounded flows by high frequency oscillation, Phys. Fluids A 4 (1992) 1605–1607.
[13] F. Waleffe, On a self-sustaining process in shear flows, Phys. Fluids 9 (1997) 883–900.
[14] K.S. Choi, J.R. DeBisschop, B.R. Clayton, Turbulent boundary layer control by means of spanwise-wall oscillation, AIAA J. 36 (1998) 1156–1163.
[15] J. Jimenez, A. Pinelli, The autonomous cycle of near-wall turbulence, J. Fluid Mech. 389 (1999) 335–359.
[16] M. Gad-El-Hak, Flow Control: Passive, Active and Reactive Flow Management, Cambridge University Press, Cambridge, MA, 2000.
[17] S. Komori, R. Nagaosa, Y. Murakami, Mass transfer into a turbulent liquid across the zero-shear gas–liquid interface, AIChE J. 36 (1990) 957–960.
[18] S. Kumar, R. Gupta, B. Banerjee, An experimental investigation of the characteristics of free-surface turbulence in channel flow, Phys. Fluids 10 (1998) 437–456.
[19] M. Rashidi, S. Banerjee, Turbulence structure in free surface flows, Phys. Fluids 31 (1988) 2491–2503.
[20] M. Rashidi, G. Hetstroni, S. Banerjee, Mechanisms of heat and mass transport at gas–liquid interfaces, Int. J. Heat Mass Transfer 34 (1991) 1799–1805.
[21] M. Rashidi, Burst-interface interactions in free surface turbulent flows, Phys. Fluids 9 (1997) 3485–3501.
[22] R.A. Handler, J.R. Saylor, R.I. Leighton, A.L. Rovelstad, Transport of a passive scalar at a shear-free boundary in fully developed turbulent open channel flow, Phys. Fluids 11 (1999) 2607–2625.
[23] L. Wang, Y.H. Dong, X.Y. Lu, An investigation of turbulent open channel flow with heat transfer by large eddy simulation, Comput. Fluids 34 (2005) 23–47.
[24] N.S. Liu, X.Y. Lu, Direct numerical simulation of spanwise rotating turbulent channel flow with heat transfer, Int. J. Numer. Method Fluids 53 (2007) 1689–1706.
[25] N.S. Liu, B.Y. Li, X.Y. Lu, Direct numerical simulation of vertical rotating turbulent open-channel flow with heat transfer, Comm. Comput. Phys. 1 (2006) 336–361.
[26] B.Y. Li, N.S. Liu, X.Y. Lu, Direct numerical simulation of vertical rotating turbulent channel flow with heat transfer, Int. J. Heat Mass Transfer 49 (2006) 1162–1175.
[27] L. Wang, X.Y. Lu, Large eddy simulation of stably stratified turbulent open channel flows with low- to high-Prandtl number, Int. J. Heat Mass Transfer 48 (2005) 1883–1897.
[28] Y.H. Dong, X.Y. Lu, L.X. Zhuang, Large eddy simulation of turbulent channel flow with mass transfer at high-Schmidt numbers, Int. J. Heat Mass Transfer 46 (2003) 1529–1539.
[29] R.J. Volino, G.B. Smith, Use of simultaneous IR temperature measurements and DPIV to investigate thermal plumes in a thick layer cooled from above, Exp. Fluids 27 (1999) 70–78.
[30] R. Verzicco, P. Orlandi, A finite-difference scheme for three-dimensional incompressible flows in cylindrical coordinates, J. Comput. Phys. 123 (1996) 402–414.
[31] R. Bergant, I. Tiselj, Near-wall passive scalar transport at high Prandtl numbers, Phys. Fluids 19 (2007) 065105.
[32] L. Wang, Numerical investigations of turbulent heat transfer and turbulence control, Ph.D. Thesis, University of Science and Technology of China, Hefei, Anhui, China, 2007.
[33] N.N. Mansour, J. Kim, P. Moin, Reynolds-stress and dissipation-rate budgets in a turbulent channel flow, J. Fluid Mech. 194 (1988) 15–44.
[34] N.S. Liu, X.Y. Lu, Direct numerical simulation of turbulent flows in a vertical rotating channel, J. Turbulence 6 (2005) 34.
[35] N.S. Liu, X.Y. Lu, A numerical investigation of turbulent flows in a spanwise rotating channel, Comput. Fluids 36 (2007) 282–298.
[36] J. Kim, P. Moin, R. Moser, Turbulence statistics in fully developed channel flow at low Reynolds number, J. Fluid Mech. 177 (1987) 133–166.
[37] R.A. Antonia, J. Kim, Turbulent Prandtl number in the near wall region of a turbulent channel flow, Int. J. Heat Mass Transfer 34 (1991) 1905–1908.
[38] H. Tennekes, J.L. Lumley, A First Course in Turbulence, MIT Press, Cambridge, MA, 1972. pp. 95–97.